Thesis for the degree of Licentiate of Engineering

Integrated Circuit Solutions for High Datarate Polymer Fiber Communication

Frida Strömbeck

Department of Microtechnology and Nanoscience
CHALMERS UNIVERSITY OF TECHNOLOGY
Göteborg, Sweden 2021

Integrated Circuit Solutions for High Datarate Polymer Fiber Communication
Frida Strömbeck

Licentiatavhandlingar vid Chalmers tekniska högskola
Technical report No. MC2-443
ISSN 1652-0769

Department of Microtechnology and Nanoscience
Chalmers University of Technology
SE–412 96 Göteborg, Sweden
Telephone + 46 (0) 31 – 772 1000

Typeset by the author using LaTeX.

Printed by Chalmers Reproservice
Göteborg, Sweden 2021

Sometimes science is more art than science, a lot of people don't get that. -Rick

Abstract

Most societies today are dependent on an Internet connection. It has to be reliable in any condition, energy efficient, but most importantly fast. High data rate communication is urgently needed, not only to connect one part of the world to the other, but also for short range applications to help us get through the day. Communication within an autonomous car, to get us from point A to point B, streaming entertainment at a Friday night, or parts of a production chain to help out at a factory. The transmitters and receivers are key components to transfer the data to make these kind of applications possible. Adjustments to what is available and possible is what challenges the progress. Fundamental limitations comes from the material properties and available energy in comparison to the noise around us. Dealing with bandwidth limitations is somewhat man-made, but the interference of different signals is completely real. Looking around for opportunities in this world leads you to look for free bandwidths. The millimeterwave-band (30-300 GHz) offers available bandwidth as well as other benefits. In this work, different circuit solutions enabling high data rate communication is proposed and presented. Different technologies are used, like state of the art processes and commercial processes. Wirebound communication through polymer microwave fiber (PMF) using energy efficient RF-DAC based modulators and power detectors (PDs) is a cheap and robust solution. In this work we explore the opportunities of short range, ultra high data rate, PMF bound communication, which is found to support 30 Gbps error free (BER$< 10^{-12}$) data.

Keywords: RF-DAC, Power Detector, Polymer Microwave Fiber, Pulse Amplitude Modulation

List of Publications

This thesis is based on the following appended papers:

Paper A. Frida Strömbeck, Zhongxia Simon He, and Herbert Zirath, *A RF-DAC based 40 Gbps PAM Modulator with 1.2 pJ/bit Energy Efficiency at Millimeterwave Band*, 2018 IEEE/MTT-S International Microwave Symposium - IMS, Philadelphia, 2018.

Paper B. Frida Strömbeck, Zhongxia Simon He, and Herbert Zirath, *Multi-Gigabit RF-DAC Based Duobinary/PAM-3 Modulator in 130 nm SiGe HBT*, The 15th European Microwave Integrated Circuits Conference (EuMIC), 2020.

Paper C. Frida Strömbeck, Mingquan Bao, Zhongxia Simon He, and Herbert Zirath, *Transmitter and Receiver Circuits for a High-speed Polymer-fiber based PAM-4 Communication Link*, submitted to –

Paper D. Frida Strömbeck, Zhongxia Simon He, and Herbert Zirath, *PAM-4 RF-DAC and PD for High Speed Polymer Microwave Fiber Communication at D-band*, submitted to –

Other Publications: The content of the following publications partially overlaps with the appended papers or is out of the scope of this thesis

Frida Strömbeck, Zhongxia Simon He, and Herbert Zirath, *AMCW Radar of Micrometer Accuracy Distance Measurement and Monitoring*, 2019 IEEE MTT-S International Microwave Symposium (IMS), Boston, 2019.

List of Acronyms

AM	–	Amplitude Modulated
AWG	–	Arbitrary Waveform Generator
Balun	–	Balanced to unbalanced
BER	–	Bit Error Rate
DAC	–	Digital to Analog Converter
DE	–	De-Emphasis
FFT	–	Fast Fourier Transform
FIR	–	Finite Impulse Response
FSPL	–	Free Space Path Loss
LNA	–	Low Noise Amplifier
MMIC	–	Monolithic Microwave Integrated Circuit
PAM	–	Pulse Amplitude Modulation
PD	–	Power Detector
PMF	–	Polymer Microwave Fiber
RRC	–	Root Raised cosine
SER	–	Symbol Error Rate
SNR	–	Signal to Noise Ratio
VCO	–	Voltage Controlled Oscillator
QPSK	–	Quadrature Phase Shift Keying

Contents

Chapter 1

Introduction

The number of internet users is steadily growing. In 2020 the number of internet users surpassed 4 billion. Fig. 1.1 shows the worldwide growth between 2005 and 2019 [7].

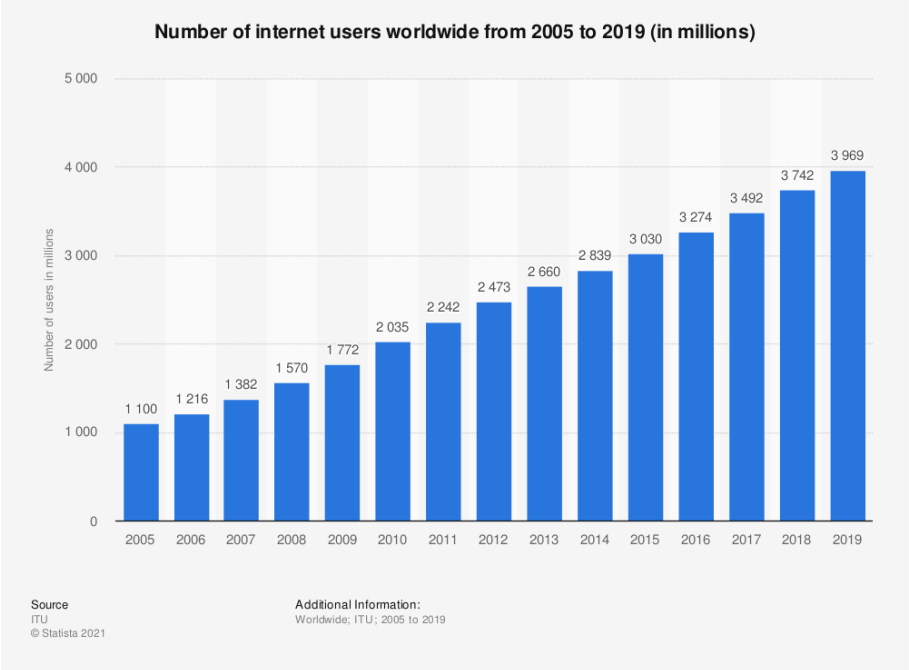

Figure 1.1: Statistics of number of Internet users worldwide.

More and more essential services for our society is heavily dependent on functional network connections and communication systems. To meet the increasing demand on the network services, new channels of communication and more efficient use of already utilized channels is vital. Different approaches are used for different applications, which is why we can see a variety of systems making up the internet.

1.1 Background

From the everyday applications using mobile phones, streaming systems and automotive cars, it is clear that high data rate connectivity even at a small distance is urgently needed. Data transfer between different central processing units (CPUs) within a local server has to be quick and reliable. Some applications require temperature stability to be used in different environments. Others are limited by power, for example battery driven devices, then power consumption becomes a major consideration.

There are plenty of benefits transmitting data at a high data rate. As long as more errors in the transmission and a higher energy consumption per bit does not occur, one can argue that there are no direct disadvantages of a higher data rate. Of course if requirements like a wider bandwidth is necessary to achieve said performance pros and cons has to be considered. Sending the same amount of information but with a higher data rate will decrease the transmission time, thus reduce the on-time of the transceiver which possibly enables a longer lifetime of the device.

What limits the amount of data that can be sent per time unit is the channel bandwidth, which in turn is limited by the response time of the active components (i.e. transistors). The response time is a consequence of the maximum frequency of oscillation of the component, so the technology is extremely important in high data rate systems. Other factors that are limiting factors are the strength of the signal in comparison to the noise of the surroundings and within the devices themselves. There is a theoretical limit of the maximum bit rate that can be transferred. In practise, the performance is always lower. The limit is given by Shannon's theorem

$$C = B\log_2(1 + \frac{S}{N}) \tag{1.1}$$

where C is the channel capacity, B is the bandwidth, S is the signal power and N is the noise power [2].

Some components that are available have a maximum oscillation frequency above 1 THz, like the 130 nm double heterojunction bipolar transistor (DHBT) developed by Teledyne [6]. In theory means that there is lots of available bandwidth. In practice there is an other story though.

The world is getting crowded, not only by people but also the radio frequency spectrum. Rules and restrictions control who can send what at which frequency band. In Fig. 1.2 a chart of different frequency allocations can be seen. There are not many free frequency bands, and bandwidths are limited. Opportunities of free bandwidths are at higher frequencies, the so-called millimeter-wave band. The millimeter-wave band is defined as frequencies between 30 GHz and 300 GHz, in other words wavelengths (in free space) from 1 to 10 mm.

If the bandwidth is limited, a higher data rate can be achieved by sending more information per symbol. For example, instead of sending either '0' or '1' one can send '00', '01', '10' or '11' in each symbol. A common way to do this is by using both amplitude and phase of the signal, but to know the phase of the signal there has to be synchronisation between the sender and the receiver (carrier recovery), hence the system becomes more complicated. These extra parts require energy to function, so a large portion of the power consumption is spent on that.

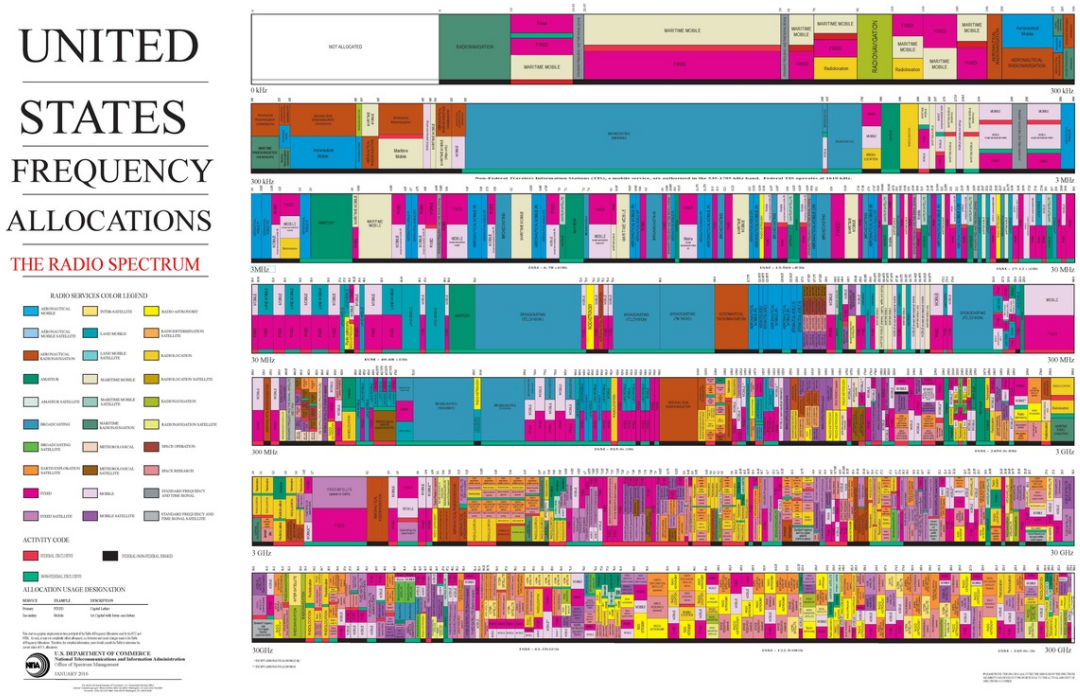

Figure 1.2: US frequency allocation.

For high data rate communication it is beneficial to move up in frequency. The components can be smaller, because the wavelength is shorter. Wider bandwidths are available and a higher resolution can be achieved.

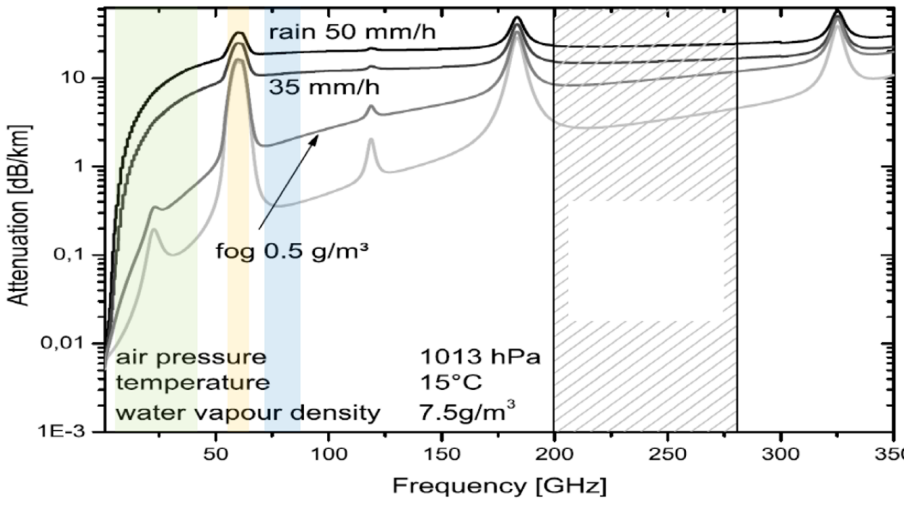

Figure 1.3: Atmospheric attenuation for different frequencies.

For wireless communication atmospheric attenuation has to be taken into consideration. In Fig. 1.3 the atmospheric attenuation for different frequencies is shown. For millimeter-wave frequencies there is a window of low attenuation between 70-175 GHz and 200-300 GHz.

1.2 Thesis Outline

Following this introduction is chapter 2, which will discuss different options to achieve high speed short range communication systems. Following that is a chapter about the technologies used in this thesis. More details of circuit designs will be presented in chapter 4, which about circuit solutions for pulse amplitude modulated communication systems. Chapter 5 focuses on system performance. In chapter 6, a conclusion of this work and future goals can be found.

Chapter 2

High Speed Short Distance Communication Systems

Both wireless communication using antennas and optical fiber communication are used today, because both systems have different advantages and drawbacks. A fiber optic system can reach far, but a wireless system is much more flexible. In this work the focus is on short range high data rate communication, thus a brief introduction of wireless communication systems will follow.

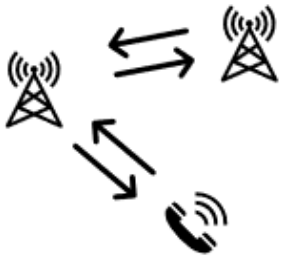

Figure 2.1

2.1 Wireless Communication Systems

A wireless communication system is made out of one part sending information using an antenna, and a transmitter (Tx), and one part receiving the information through an antenna, and a receiver (Rx). The signal is by definition not wirebound between the antennas. The strength (power) of the signal that is received depends on the power of the signal that was sent, the directivity (i. e. how much spreading of the signal that occurs) of the antennas, and the loss that occurs due to the spreading of the signal (free space path loss).

Friis' transmission equation helps calculating the amount of power that gets transmitted from one antenna to the other.

$$P_r = \frac{G_t G_r P_t}{\text{FSPL}} \tag{2.1}$$

P_r is the received power, P_t is the transmitted power, G_t is the antenna gain of the transmitting antenna, G_r is the antenna gain of the receiving antenna, and $FSPL$ is the free space path loss. The free space path loss can be calculated using

$$\text{FSPL} = (\frac{4\pi df}{c})^2 \tag{2.2}$$

where d is the distance, f is the frequency and c is the speed of light. What limits the transmission is usually noise, primarily thermal noise from the receiver and the loss of the antenna.

The thermal noise power at the input of the receiver is given by;

$$N_0 = kTB \tag{2.3}$$

where k is Boltzmann's constant, T is the temperature of the antenna (which is the temperature of the object is is pointed at), and B is the bandwidth of the signal.

Signal to noise ratio (SNR) is a common measure within wireless communications. It is defined as;

$$\text{SNR} = \frac{P_{in}}{N_0} = \frac{E_b}{n_0}\frac{R_b}{B} \tag{2.4}$$

where $N_0 = n_0 B$ is the noise power and $E_b R_b$ is the digital signal power. Further more, $\frac{R_b}{B}$ is the spectral efficiency.

The noise that is contributed by the component makes the SNR lower at the output of said component. The change in SNR is defined as the noise figure (NF) of the component.

$$NF = \frac{\text{SNR}_{\text{in}}}{\text{SNR}_{\text{out}}} \tag{2.5}$$

For a cascaded circuit the total noise figure is given by Friis' formula for noise;

$$NF = F_1 + \frac{F_2 - 1}{G_1} \tag{2.6}$$

where F_1 is the noise figure of the first component, G_1 is the gain from the first component, and F_2 is the noise figure from the second component [3].

The symbol error rate depends on the SNR. A larger SNR gives a smaller symbol error rate. A symbol can contain one or many bits, depending on the spectral efficiency of the modulation format.

Of course the goal is to get error free communication, which is why the noise should be kept low. For a larger bandwidth, more thermal noise gets picked up by the receiver. At the same time, a large bandwidth means there can be a lower complexity of the modulation format (to obtain same data rate). A lower complexity in the modulation, means it is less sensitive to noise, which is why it requires a smaller SNR to remain error free.

The other part of the SNR is the signal strength. Sending a strong signal is very beneficial, though not always easy. As the carrier frequency gets higher, power is becoming a critical problem to obtain. The directivity of the antennas gets more

important for the signal to not spread out, thus fade in strength. As the beam becomes smaller, the alignment between the antennas becomes increasingly difficult. The overall system will be more sensitive to vibrations and small effects that can cause miss-alignment.

For short range systems that require robustness wirebound communication can be beneficial.

2.2 Polymer Microwave fiber

Polymer microwave fibers (PMF) offer lots of benefits for short range communication systems. The PMFs are flexible and made of low cost plastics. Compared to optical fibers the alignment to the PMF is much simpler, because of the larger size of the PMF, which is why the PMF is a more robust solution. Furthermore, since the signal is mostly confined in and around the PMF there are no legal frequency restrictions (due to the frequency allocation restrictions), which either limits the data rate or requires high modulation schemes, thus require high complexity. A higher complexity usually leads to high cost and high power consumption.

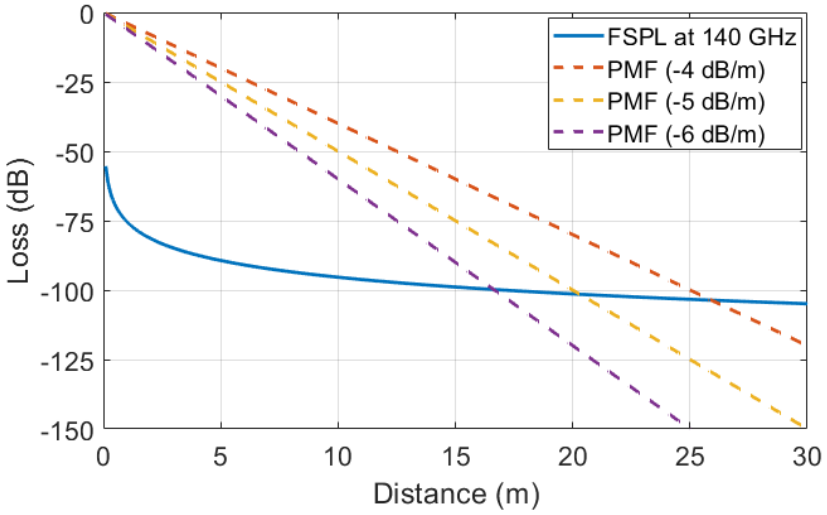

Figure 2.2: FSPL at 140 GHz compared to PMFs with 4,5 and 6 dB loss per meter.

Comparing short range communication over PMF with air, for shorter distances the loss is less in the PMF which can be seen in Fig. 2.2.

An example of a PMF that was used during some measurements in this work was provided by Lehrstuhl für Hochfrequenztechnik (LHFT), Germany. A photo of the D-band (110-170 GHz) dielectric waveguide can be seen in Fig. 2.3. The length of the fiber is 1 meter and it has a rectangular solid cross section (1 mm by 2 mm), and is made out of high-density (with a density above 0.930 g/cm^3) polyethylene (HD-PE). Examples of other polymers that can be used are polystyrene (PS), polytetrafluoroethylene (PTFE) and polypropylene (PP) [13].

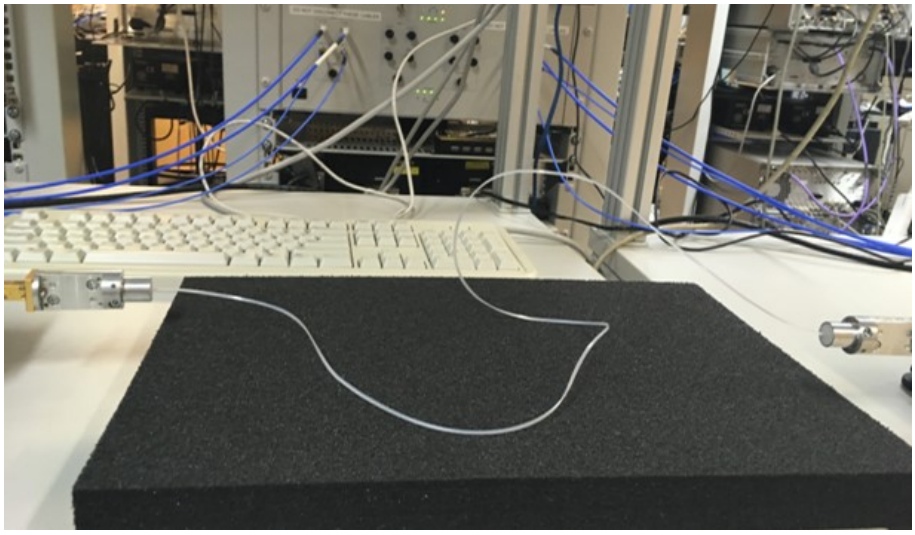

Figure 2.3: A 1 meter PMF with a solid rectangular cross section (1 mm by 2 mm).

Measurement of the S parameters (S11 and S21) of the fiber in Fig. 2.3 can be seen in Fig. 2.4. The measurement include the loss of the transition to the waveguide on both sides.

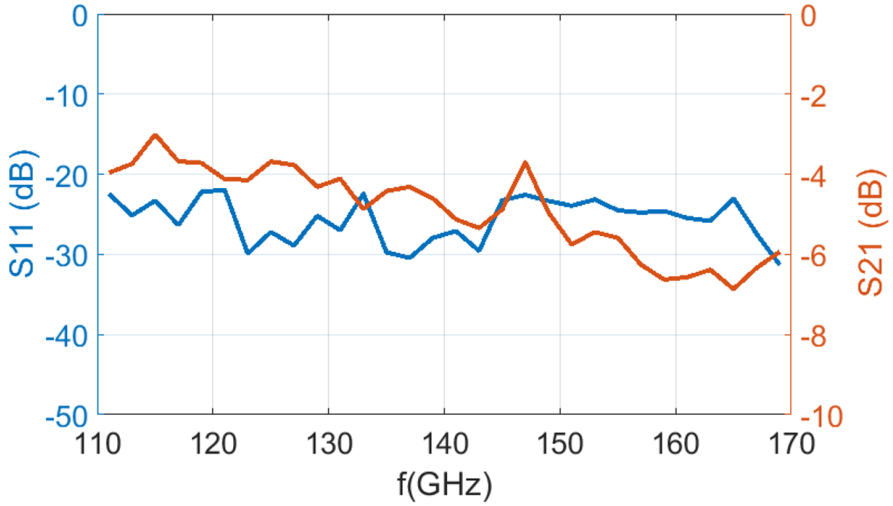

Figure 2.4: Measured S21 and S11 for the fiber, including the waveguide transitions.

One of the challenges with communication over PMF is the group delay, or more importantly the difference in group delay for different frequencies. This degradation of the signal is called dispersion.

In Fig. 2.5 the group delay of the measured fiber in Fig. 2.3 is shown.

The difference in group delay between 110 GHz and 170 GHz is about 0.6 ns (in Fig. 2.5). For higher data rates with a wide bandwidth, this has to be handled in some way. De-emphasis and equalization are some ways to deal with this which will be mentioned more in Section 2.4.

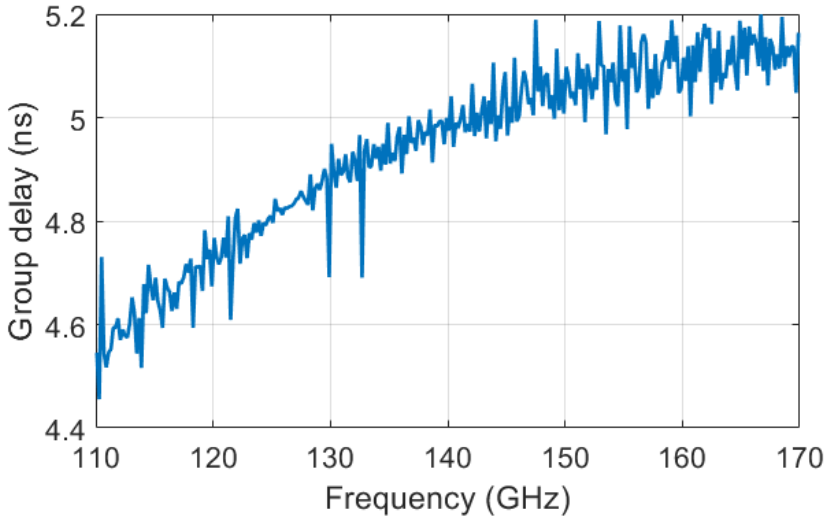

Figure 2.5: Measured group delay in the D-band.

Looking at modulation formats that reduce the bandwidth (less sensitive to dispersion), while still keeping the simplicity, pulse amplitude modulation becomes a candidate.

2.3 Pulse Amplitude Modulation

Pulse Amplitude Modulation (PAM) can be either unipolar or bipolar. For a unipolar signal all levels are non-negative, while a bipolar signal has evenly distributed levels where half of them are negative and half of them are positive. A bipolar signal uses a single side band, but requires carrier recovery. A unipolar signal can use both side bands, and a simple power detector is sufficient to demodulate the signal.

The transmitted unipolar PAM signal over one symbol period ($0 \leq t \leq T$) is given by

$$s_i(t) = A_i g(t) \sin(2\pi f_c t) \tag{2.7}$$

where $A_i = (i-1)d, i = 1, 2, 3...M$ for unipolar M-PAM, d is the amplitude separation distance between different levels, $g(t)$ is a real-valued pulse shaping function, and f_c is the carrier frequency.

The symbol error probability for coherent unipolar M-PAM is given by;

$$P_s = \frac{2(M-1)}{M} Q\left(\sqrt{\frac{3(\log_2 M)E_b}{(2M^2 - 3M + 1)N_o}}\right) \tag{2.8}$$

where $Q(\sqrt{2}x) = \frac{\text{erfc}(x)}{2}$. Note that erfc is referring to the complementary error function [5].

The symbol error probability for incoherent unipolar M-PAM is given by;

$$P_s = \frac{1}{M}\left[\exp\Big(-\frac{1}{2}(\log_2 M)B_M \frac{E_b}{N_o}\Big) + (2M-3)Q\left(\sqrt{(\log_2 M)B_M \frac{E_b}{N_o}}\right)\right] \tag{2.9}$$

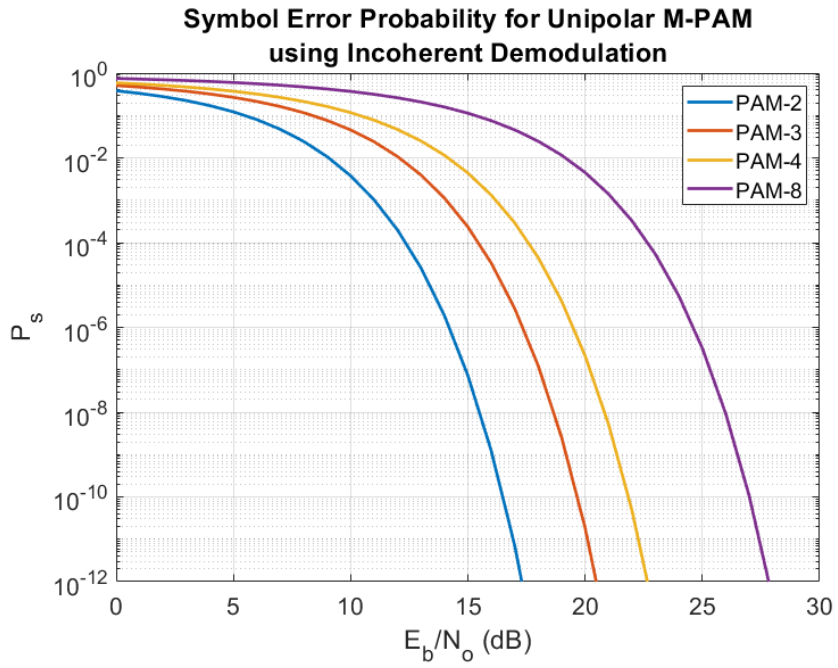

Figure 2.6

where B_M is given by;

$$B_M = \frac{3}{2M^2 - 3M + 1} \tag{2.10}$$

The difference between coherent and non-coherent demodulation becomes negligible when M becomes large.

While PAM-4 uses four different power levels, the ideal power levels are distributed in such way that a most significant bit (MSB) has double the power of the least significant bit (LSB).

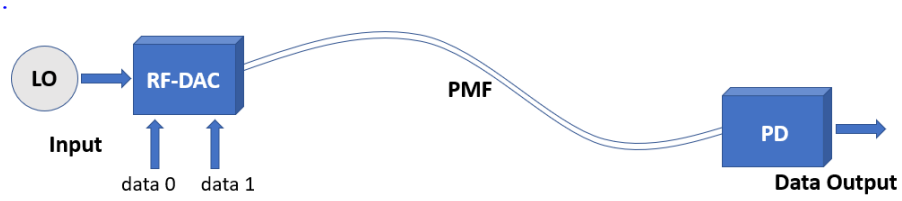

Figure 2.7: Using new technology to enable high data rate, using simple, and in return energy efficient systems is key in the PMF linked channel.

2.4 System Simulation

The effects of the fiber on the PAM-4 signal was simulated to understand the limitations and important parameters of the system. Matlab was used for the system simulations, and CST Studio Suite was used to simulate the fiber. The electromagnetic (EM) simulation showed the propagation of the signal (Fig. 2.8). A

scattering (S) parameter file was created which was used to predict the effects of the PAM-4 signal.

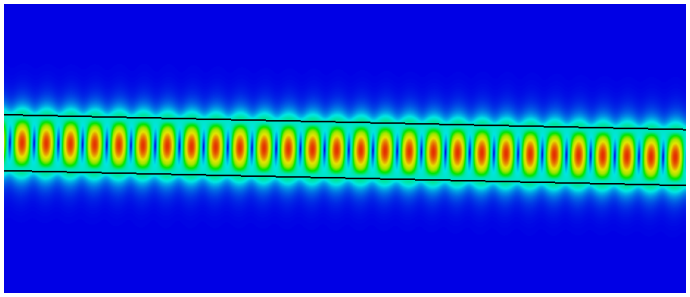

Figure 2.8: CST was used to simulate the propagation of the signal through the fiber at D-band. The frequency was set to 140 GHz in this figure.

Polytetrafluoroethylene (PTFE) was used as material of the fiber and the dimensions were 1x2mm in the simulation. Simulated S21 and group delay can be seen in Fig. 2.9 and Fig. 2.10. The simulations of the fiber did not include any transition to and from the fiber.

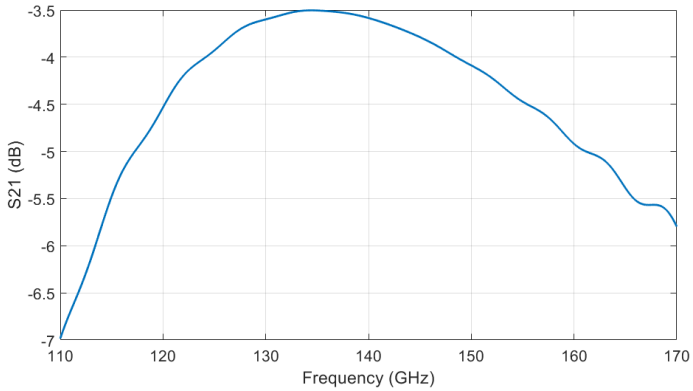

Figure 2.9: CST simulated S21 of a 1 meter long PTFE fiber.

Random data (D) is generated and up-sampled. An oversampling of 400 per symbol was used during these simulations. The data was given an amplitude in voltage (A_{V}), a constant amplitude of leakage (A_{l}) was added, which is independent to the data. The amplitude is multiplied with the sinusoidal carrier, resulting in a modulated signal (y).

$$y = (A_{\mathrm{l}} + A_{\mathrm{V}} D)\sin(2\pi f_c t) \tag{2.11}$$

The signal is converted to frequency domain using fast fourier transform (FFT), and the transfer function generated from the s-parameters of the PMF is applied to the signal. The signal is then converted back to time domain, using inverse FFT. The envelope of the output signal is down-sampled, and the amplitude is compared to recover the output bitstream.

Simulations with a carrier frequency of 135 GHz, where the attenuation is the lowest, and the difference in attenuation over the bandwidth of the signal is minimized,

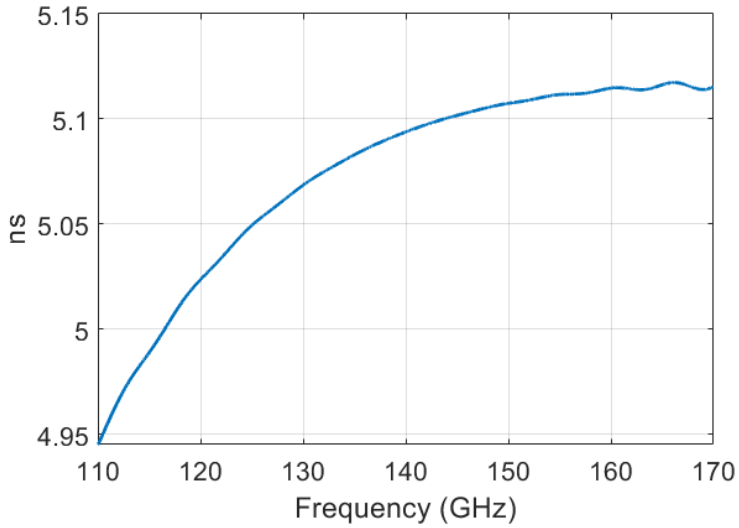

Figure 2.10: CST simulated group delay of a 1 meter long PTFE fiber.

was compared to simulations with 150 GHz as the carrier, where the group delay difference is significantly lower over the bandwidth of the signal. The eyediagrams of the demodulated PAM-4 signal for the different carrier frequencies can be seen in Fig. 2.11. The Baudrate was 10 GBd for both carriers, and the fiber was 1 meter long.

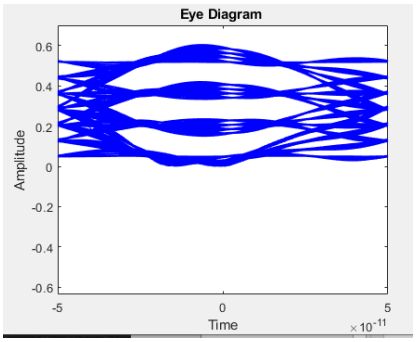

(a) Eyediagram of a demodulated 10 GBd PAM-4 signal using a carrier at 135 GHz over the simulated 1 meter long fiber.

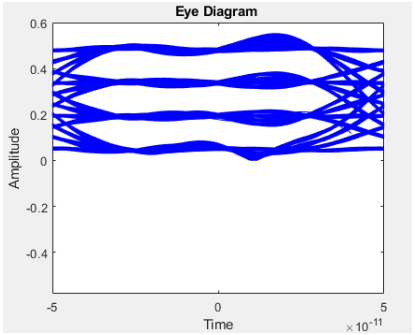

(b) Eyediagram of a demodulated 10 GBd PAM-4 signal using a carrier at 150 GHz over the simulated 1 meter long fiber.

Figure 2.11: Eyediagrams of a demodulated transmissions over 1 meter pmf. The amplitude unit is volt, and the time unit is seconds.

The difference in the shape of the eyediagrams are noticeable. The lower carrier frequency has more widening of the eyediagram, due to the difference in group delay. To get a clearer view of the effects, same simulations were made, but over a 2 meter long fiber. The eyediagrams can be seen in Fig. 2.12.

The difference in group delay for different frequencies (dispersion) of the fiber is a critical limitation. From the simulations one can see that the dispersive effects are lower at high carrier frequencies for the PMFs. From that point of view, it is beneficial to use a high carrier frequency. Further more, moving up in frequency face

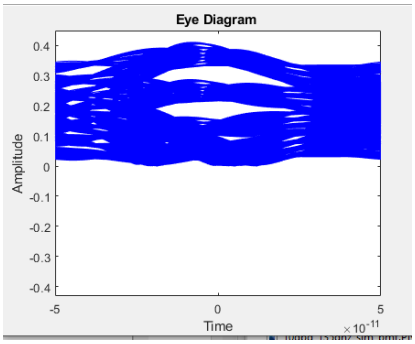

(a) Eyediagram of a demodulated 10 GBd PAM-4 signal using a carrier at 135 GHz over the simulated 2 meter long fiber.

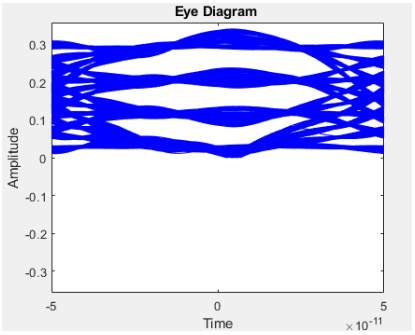

(b) Eyediagram of a demodulated 10 GBd PAM-4 signal using a carrier at 150 GHz over the simulated 2 meter long fiber.

Figure 2.12: Eyediagrams of a demodulated transmissions over 2 meter pmf. The amplitude unit is volt, and the time unit is seconds.

other challenges, like power limitations.

2.4.1 Pulse shaping

The fiber changes the shape of the signal, and the ideal output signal has the shape of the input signal. If the input signal is used as output and the inverse transfer function (of the fiber) is used to calculate the input, the ideal input signal can be retrieved. In Fig. 2.13 the shape of the simulated input signal can be seen. The carrier used in the simulation is 150 GHz and the bit rate is 15 Gbps PAM-2 signal.

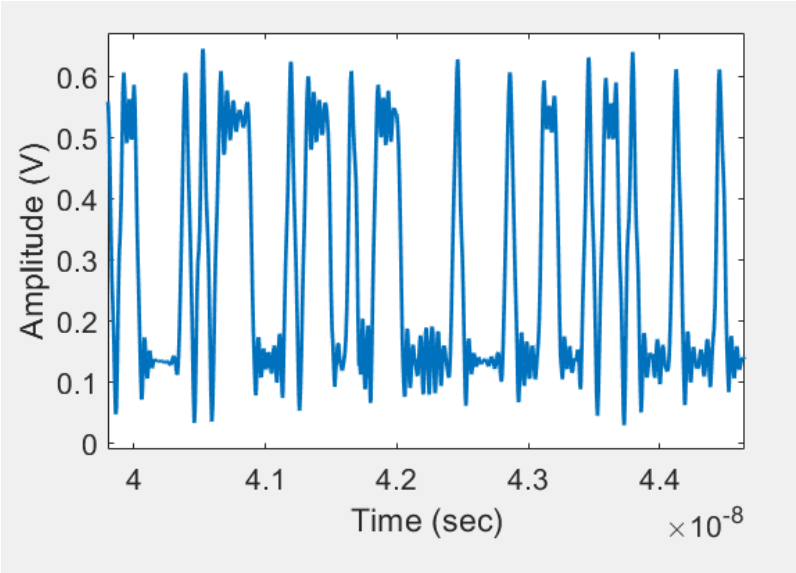

Figure 2.13: Using the inverse transfer function of the fiber to achieve the ideal input signal. The data rate is 15 Gbps and the carrier frequency during the simulation is 150 GHz.

The lower frequencies are attenuated, giving a sharper edge if the bit is switched.

De-emphasis can be used on the transmitter side to achieve this effect, and the pulse shaping using one negative post cursor tap can be seen in Fig. 2.14.

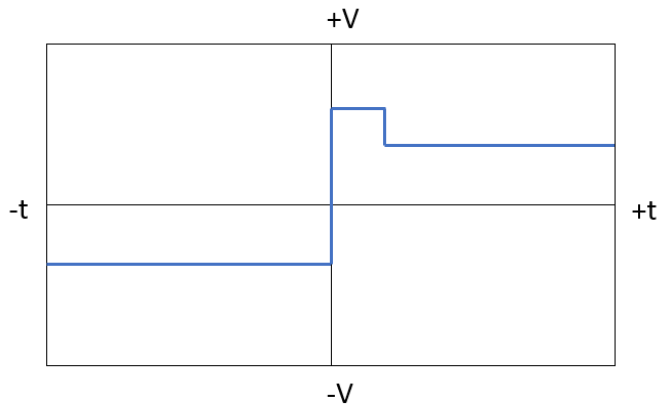

Figure 2.14: De-emphasis with one negative post cursor tap.

Compensation for the distortion of the signal can also be done at the receiver side, using an equalization filter (equalizer). The easiest implementation of an equalizer is a high pass filter, that will attenuate the lower frequencies of the signal, and in that way equalize the signal.

Chapter 3

Millimeterwave MMIC Technologies

In this work mainly two different technologies has been used, one developed by Teledyne scientific company and the other by Infineon technologies.

3.1 250 nm InP DHBT Technology

Teledyne Scientific Companies Indium Phosphide (InP) heterojunction bipolar transistor (HBT) process TSC250 is an advanced bipolar process that relies on sub-micron transistor scaling to achieve a state-of-the art device performance. Devices in the technology offer typical RF figures-of-merit (f_t and $f_{\max}$) of 350/600 GHz while maintaining a common-emitter breakdown voltage (BV_{CEO}) of greater than 4V. The wide bandwidth and high power handling capability of the devices make the technology ideally suited for next generation millimeter-wave, mixed-signal and digital integrated circuits.

The technology has 4 metal layers, M1, M2, M3 and M4. The dielectric constant of the interlayer dielectric (BCB) is estimated to be $\epsilon_r = 2.7$. A cross-section drawing can be seen in figure 3.1.

Using a thin layer of Silicon Oxide (SiO), that sits on the InP substrate, thin-film resistors are formed. The metal-insulator-metal (MIM) capacitors are formed between M1 and the capacitor metal (CAPM) with a 200 nm Silicon Nitride (SiN) dielectric layer in between.

Each layer has a maximum current density that cannot be exceeded. Metal 1 has 4mA/μm, metal 2 and 3 has 5mA/μm, metal 4 has 15mA/μm and the thin-film resistor has 1mA/μm. The vias connecting different layers also has limits for the current.

The design kit includes two types of transistors; standard devices, and single-sided collector contact devices. The single-sided collector device has a collector contact on only one side of the base mesa. This results in approximately a 2x increase in the collector resistant, but reduces the footprint of the transistor by approximately 30%. The estimated safe operating area for the devices can be seen in 3.2.

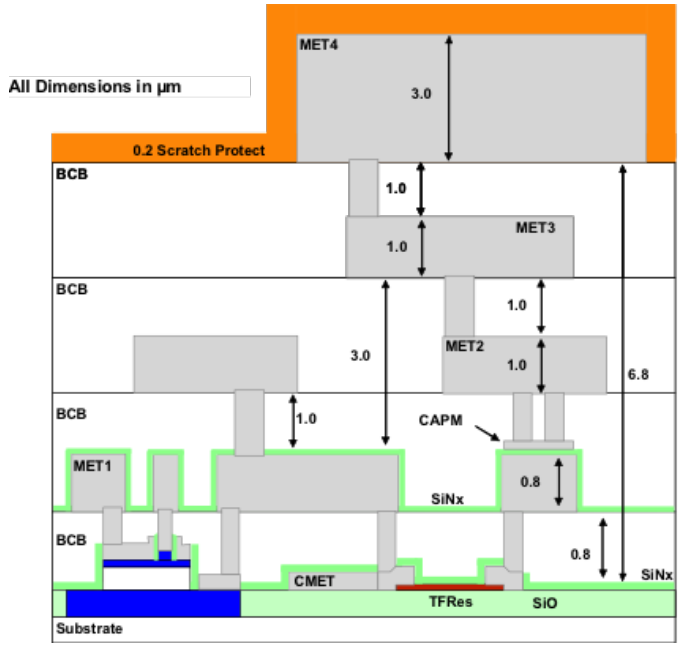

Figure 3.1: Representative cross-section of TSC250 IC technology. Drawing is not to scale. *Courtesy: Teledyne Scientific Company*

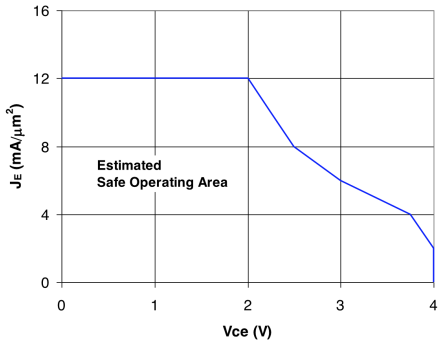

Figure 3.2: Estimated safe operating area for 250nm HBT devices in common-emitter configuration. The current density is given by $J_E = \frac{I_C}{(0.25 \times \text{Emitter length})}$. *Courtesy: Teledyne Scientific Company*

A design kit for TSC250 was available for ADS to simulate the predicted performance.

3.2 130 nm SiGe BiCMOS Technology

The Silicon Germanium (SiGe) BiCMOS technology consists of two different transistor types, the hetrojunction bipolar transistor (HBT) and the complementary metal oxcide semiconductor (CMOS) transistor. CMOS enables low power logic operation, while the HBTs is for high speed analog components. Infineon's 130 nm SiGe BiCMOS process that is used in this work includes npn transistors with $f_t/f_{\max}$ of 250/400 GHz. A cross-section of the technology can be seen in Fig. 3.3. The

technology also include thin film resistors, metal-insulator-metal (MIM) capacitors, junction capacitors, pin diodes and six layers of copper based interconnects (M1-M6). M1-M4 are thinner layers compared to M5-M6 which are used as the top layer of the microstrip lines for RF routing. M4 is used as the ground layer in most cases (some passive components like phase shifters may use another ground layer). A single base high speed npn transistor with an emitter mask size of 0.22x2.8 μm^2 exhibits a common-emitter breakdown voltage (BV_{CEO}) of 1.4 V.

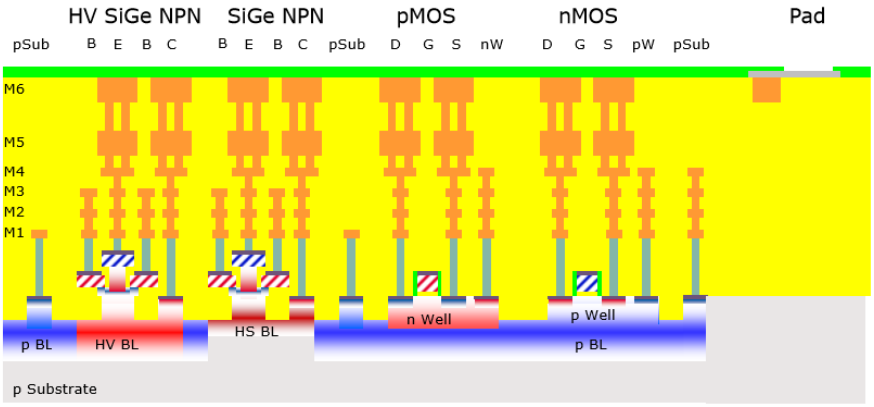

Figure 3.3: Cross-section of Infineon's B11HFC technology. *(Courtesy: Infineon technologies)*

A design kit for B11HFC was available for Cadence to simulate the predicted performance.

Chapter 4

Circuit Solutions for PAM Modulated Communication Systems

Looking at some of the possible parts of a PAM communication system a local oscillator (LO) is required. It can either oscillate at the carrier frequency of the system or an X-times lower frequency and be followed by a frequency multiplier or a sub-harmonic mixer. At higher frequencies it is challenging to achieve oscillators with high output power. Off-chip oscillator can be used, but then there is a challenge to transfer the signal to the chip.

A radio-frequency digital-to-analog converter (RF-DAC) can be used as a PAM modulator. The RF-DAC uses an LO at desired carrier frequency and modulates the power depending on the data bits that are applied to the RF-DAC. For PAM-4 the RF-DAC uses two data input ports and modulates the signal to four different power levels. A power amplifier (PA) can follow the output of the RF-DAC.

The transition from the chip to the PMF, and from the PMF to the chip is an important part of the system. Several different solutions are presented in [12] [19] [16] [15].

On the receiver side, the first stage can be a low noise amplifier (LNA). The demodulation is in part done a power detector (PD), which delivers an output voltage corresponding to the power that is fed at the input. For a PAM-4 signal four different voltages, one for each possible symbol, is received. To be able to receive a single bit stream one can use comparators.

In this chapter the focus will be on the RF-DAC and the PD.

4.1 Emitter coupled pair RF-DAC

For high-speed solutions current steering is the most commonly used technique to create an "On-Off"-switch. This can be done by using a differential pair [18].

To enable low power operation, the design topology adopts emitter coupled pair (ECP) as a gain control. By using two of such ECP structure, the local oscillator (LO) input can be converted into PAM modulated millimeterwave output. The ECP

structure can regulate the output amplitude at a high switching rate (high data rate) as well as ensure good output linearity for PAM operation.

In Paper A an RF-DAC based PAM-4 modulator was designed and fabricated in the TSC250 InP technology. The frequency range for the circuit covered E-band (60-90 GHz) The simplified schematic of the proposed modulator is illustrated in Fig. 4.1. Two ECP structures are used for most significant bit (MSB), D0, and the least significant bit (LSB) D1 respectively. The ECP for MSB includes transistor E1-E4 (transistor size: 3 μm for E1 and E4, 8 μm for E2 and E4), and the transistors E5-E8 (transistor size: 3 μm for all) are used for LSB. The LO input signal is given at the base of E1 and E5, while both E1 and E5 are configured as emitter followers, R7=R9=100 Ohm are used to achieve wide band matching after power split.

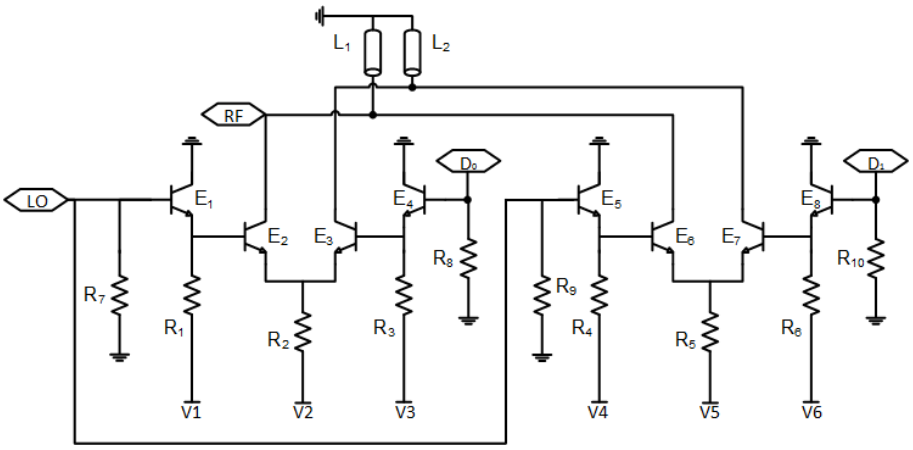

Figure 4.1: A simplification of the schematic that is used for the RF-DAC

The design of the RF-DAC is based on using differential pairs as a way to control the output power of the signal. When MSB bit '1' (0 V as logic '0' and 0.3 V as logic '1') is presented at the base of E4, it would steer the current away from E2 therefore reduce the output amplitude. Similar mechanism is applied to the other ECP, however with scaling of the transistor E6 and E7 act as LSB. The collectors of E2 and E6 are connected and shared a common inductor L1 (realized by a 240 μm microstrip line) to generate RF output. The photo of the fabricated MMIC is shown in the Fig. 4.2.

Time domain measurements using a Lecroy LabMaster 10-100Zi real-time oscilloscope to capture output RF signal, demonstrated capability to transmit a PAM-4 signal at data rates up to 40 Gbps. At 40 Gbps the bit error rate (BER) was measured to be 3.7×10^{-6}, and the dc energy efficiency was 1.2pJ/bit. The peak output power of the RF-DAC was measured to be -5 dBm at 75 GHz.

In Paper C a similar design was used, but shifted to F-band (90-140 GHz). Instead of using transistor scaling, to create a MSB and LSB, complete symmetry was used, but different emitter voltages for the pairs were used (1.7V vs 2.8V). A photo of the RF-DAC based PAM-4 modulator can be seen in Fig. 4.3. The LO input signal is applied on the right side and the RF output signal is delivered at the left side of the chip. DC bias is applied on the top, while the two data input ports

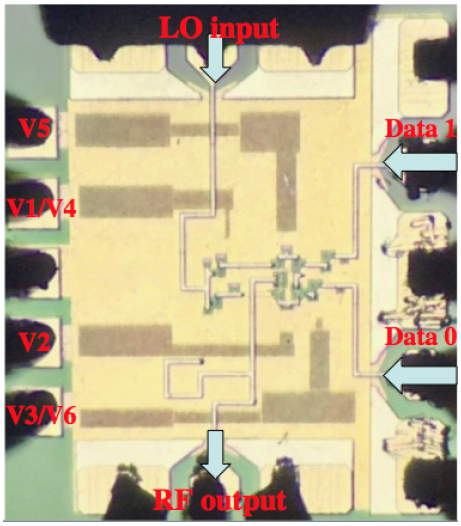

Figure 4.2: The photo of the RF-DAC. The chip size is 800μm x 800μm.

are located at the bottom. The total size of the MMIC including pads is 0.55 mm^2, and 0.29 mm^2 without pads.

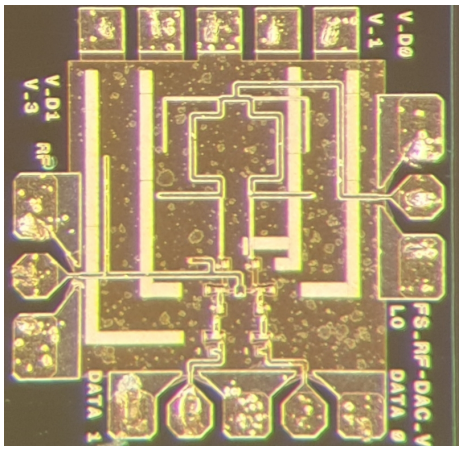

Figure 4.3: A micrograph of the fabricated RF-DAC. The chip size including pads is 740 μm by 740 μm.

The PAM-4 modulator was measured in frequency domain, on-wafer, using a MPI TS200 probe station. The output S21 measurement was captured with a Anritsu VectorStar ME7838A vector network analyser (VNA). A frequency sweep from 70 GHz to 130 GHz and 130 GHz to 170 GHz can be seen in Fig. 4.4. The four different traces represents the four different input data states of the PAM-4 modulator. The highest level is corresponding to data input '00', while the lowest level correspond to data input '11'. The -3dB bandwidth is between 87 GHz and 130 GHz, resulting in a 43 GHz wide band -3dB bandwidth. The difference in power between the highest power level '00' and the lowest power level '11' is approximately 10 dB for frequencies between 90-145 GHz.

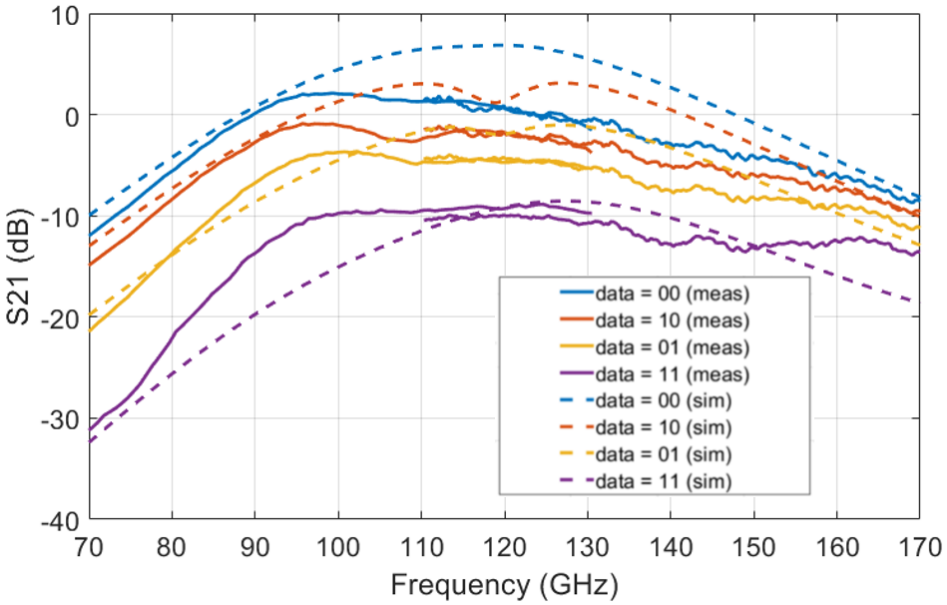

Figure 4.4: S21 for the different digital data input. LO is port 1 and RF is port 2. The measured results are shown in the solid lines and the simulated results in the dashed lines. The LO input power is -6 dBm.

4.1.1 Duobinary/PAM-3 Modulator

In Paper B; three power level states where used instead of four. Three levels can be used for duobinary modulated data or PAM-3 modulated data. Duobinary modulation as an alternative modulation format of higher spectrum efficient and moderate linearity requirement, has been studied in [9].

With a binary encoder similar to that presented in [10] [11], binary input bits are coded into 3-power-level symbols that yields 1.6 bps/Hz spectrum efficiency. An RF-DAC can be used after the encoder to directly generate such PAM-3 output at desired frequency.

For PAM-3, the modulator uses three-valued logic (ternary), with three unipolar states (’0’,’1’, and ’2’). To create these states either both data ports are "off" representing ’0’, one data port is "off" and one is "on" representing ’1’, or both data ports are "on" representing ’2’.

For duobinary, the modulator also uses three states (’-1’, ’0’, ’1’). Either both data ports are "off" representing ’-1’, one data port is "off" and one is "on" representing ’0’, or both data ports are "on" representing ’1’.

Applying voltage at the data input port attenuates the output signal. The voltage applied results in a corresponding attenuated output signal.

The circuit designed in this project had a bandwidth from 35 GHz to 130 GHz. A photo of the circuit can be seen in Fig. 4.5.

The circuit was tested in time domain, using a Lecroy LabMaster 10-100Zi real-time oscilloscope to capture output RF signal, and demodulating it. PAM-3 data transmission with a bit rate of 28 Gbps was demonstrated with a symbol error rate

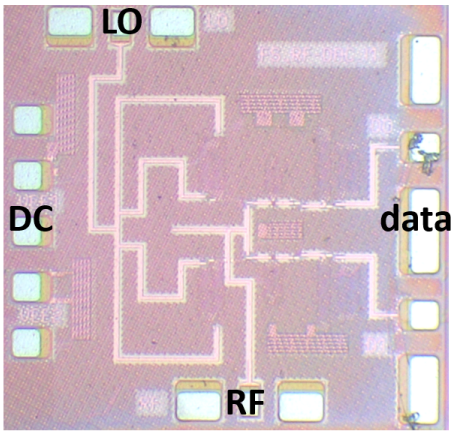

Figure 4.5: A micrograph of the modulator. The size including the pads is 800 μm by 800 μm.

of $1.4 * 10^{-6}$ (Fig. 4.6a). Using duobinary modulation data transmissions up to 30 Gbps was demonstrated with a SER of $6.4 * 10^{-6}$ (Fig. 4.6b).

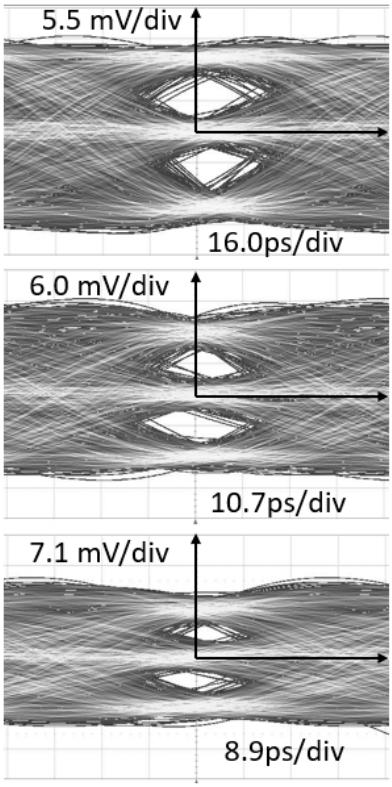

(a) PAM-3

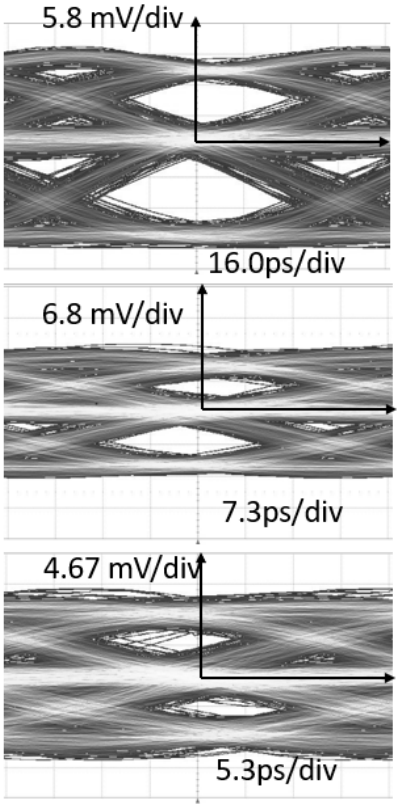

(b) Duobinary

4.2 Stacked RF-DAC

Another topology that were investigated is a stacked transistor design. The collector of one transistor is connected to the emitter of the other transistor, and the data is applied at one of the transistor's base, while the LO is applied at the other transistor's base. Early investigation showed that this topology has low DC power consumption.

In Fig. 4.7, there is a photograph of the first version of the stacked RF-DAC, made in the 250 nm Teledyne process and operating in E-band.

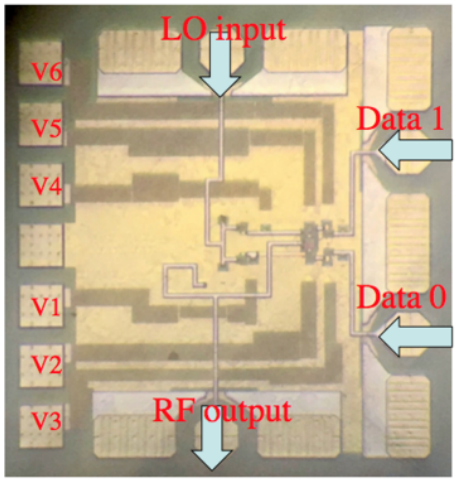

Figure 4.7: A micrograph of the stacked E-band modulator. The size including the pads is 800 μm by 800 μm.

The circuit consumes 18 mW DC power, and demonstrated data rates up to 25 Gbps.

In Paper D, a new version of the stacked RF-DAC was tested, using the Infineon b11 process. A simplified schematic of the circuit can be seen in Fig. 4.8.

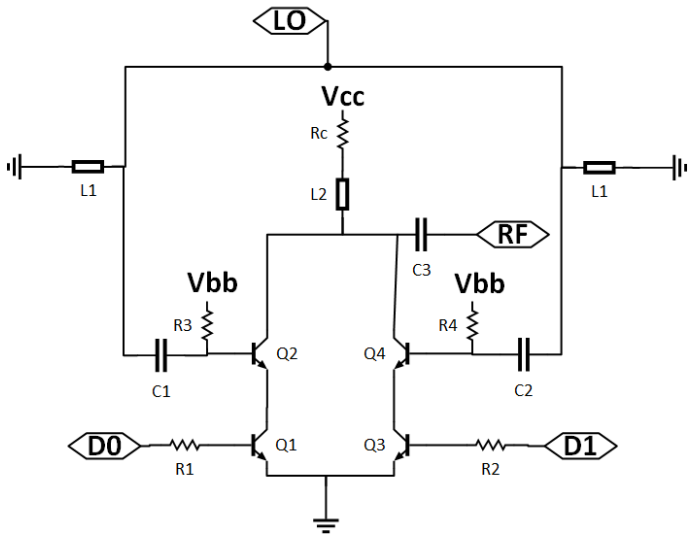

Figure 4.8: A simplified schematic of the RF-DAC

The circuit was designed to cover D-band and includes a frequency multiplier as well as an amplifier.

This circuit was also measured on-wafer using a probe station. The output power, for different data input, was captured with a Keysight PNA-X (67 GHz N5247A). The input power to the LO-input was 5 dBm and was swept between 55 and 85 GHz. A VDI extender WR-12 was used to provide the input signal. The output power for different data input, both simulated and measured, can be seen in Fig. 4.9.

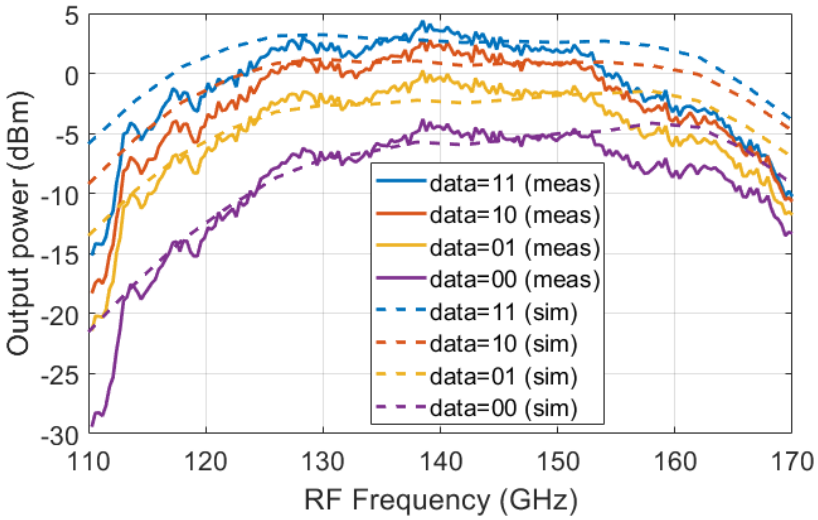

Figure 4.9: Output Power for different output frequencies at 5 dBm LO input. Solid lines represent the measurements, while the dashed lines are the simulated values.

4.3 Power Detectors

The receivers used for PAM in this work is based on power detectors (PD). Some of the important parameters for a PD is sensitivity, linearity and responsitivity. The output voltage change should happen fast, which means that higher frequencies should have a chance to pass, while filtering out the carrier. Using a low pass filter at the output will instantly increase the response time, so it is not suitable for high data rate communication. A way to deal with suppression of the carrier is to use a balanced topology. A balun can be used to split the input signal in two, with a 180 degree phase difference (for the carrier). The leakage of the carrier will cancel each other at the output. In work by [1], both hybrids and baluns were used to suppress different harmonics of the carrier.

In this work, PDs with a passiv balun or active balun are evaluated.

The passive balun was implemented as a folded Marchand balun. The ground plane is lowered to reduce the losses. The input is on the higher level metal, which is left open at the end. The two outputs are shorted in opposite end, and are on a metal below the top input metal.

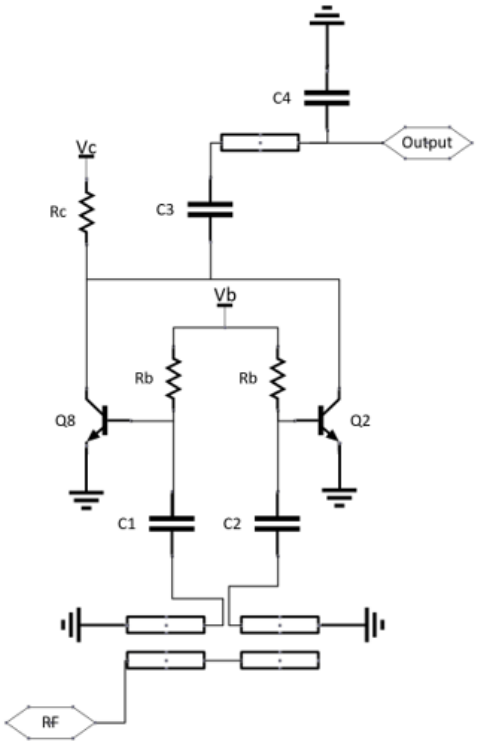

Figure 4.10: Simplified schematic of the topology used for the PD using a passive balun at the input.

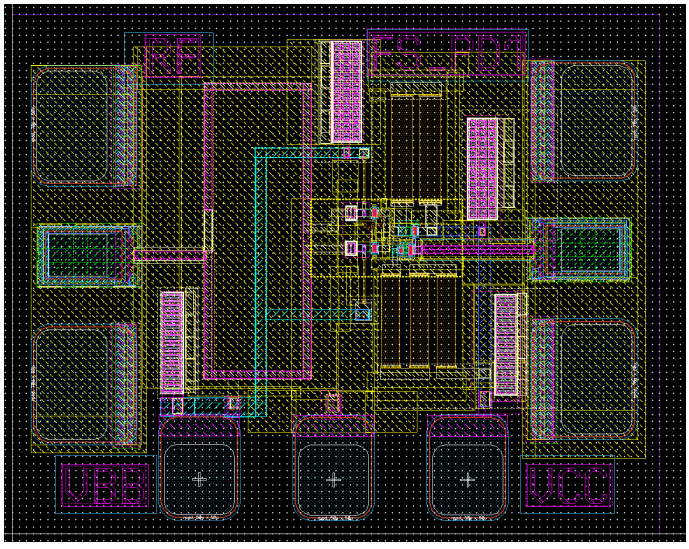

Figure 4.11: Layout of the PD with a folded Marchand balun in Infineon's B11HFC

Amplifiers can be added both at the input and output depending on the requirements of the system.

The passive Marchand balun can be changed to an active solution.

As shown in Fig. 4.12, a common-emitter configured transistor, Q1, and a

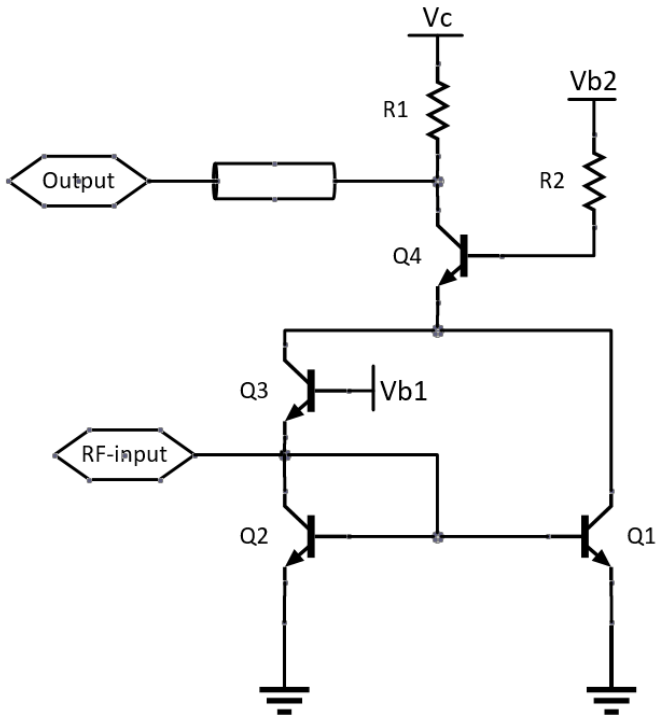

Figure 4.12: Simplified schematic of the topology used for the PD with an active balun

common-base configured transistor, Q3, are used as nonlinear components for power detectors. Their collector currents are added and applied at the stacked transistor Q4, to amplify the output signal. The output of the power detector is taken at the collector of Q4. The collector and base of Q2 are connected to form a diode which provides a DC path for Q3, and DC-bias for Q1.

The collector current of a transistor is given by a Taylor expansion

$$I_{\mathrm{c}} = a_0 + a_1 V_{be} + a_2 V_{be}^2 + ... \tag{4.1}$$

where a_0 is a function of amplitude of V_{be} in an ideal case, V_{be} for common emitter configured transistor is equal to $-V_{be}$ for common base configured transistor.

The single-ended input signal is applied at the base of Q1 and the emitter of Q3 simultaneously. Due to the transistor's nonlinearity, the outputs of Q1 and Q3 contain DC component and harmonics. The odd-order harmonics at the Q1 and Q3's outputs are 180 degree out of phase, since the transistor Q1 is common-emitter configured and Q3 is common-base configured. Thus, connecting Q1 and Q3's outputs, the odd-order harmonics will be suppressed. The desired function of Q4 is amplification of the data signal, which is why a relatively large device is selected to get sufficient gain. Due to parasitic the device will have a lower gain for the RF-signal, which will help to suppress undesired fundamental and higher order harmonics.

In paper D the PD was integrated with an amplifier at the input. The fabricated PD can be seen in Fig. 4.13.

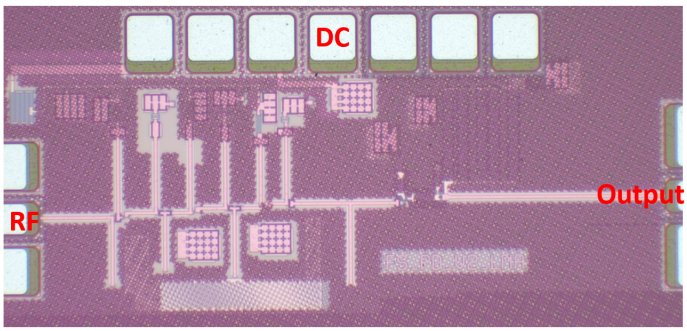

Figure 4.13: Micrograph of the PD.

Simulated output voltage in time domain can be for corresponding input signal can be seen in Fig. 4.14. The carrier frequency was 130 GHz and the datarate was 20 Gbps. The simulation was done using Cadence.

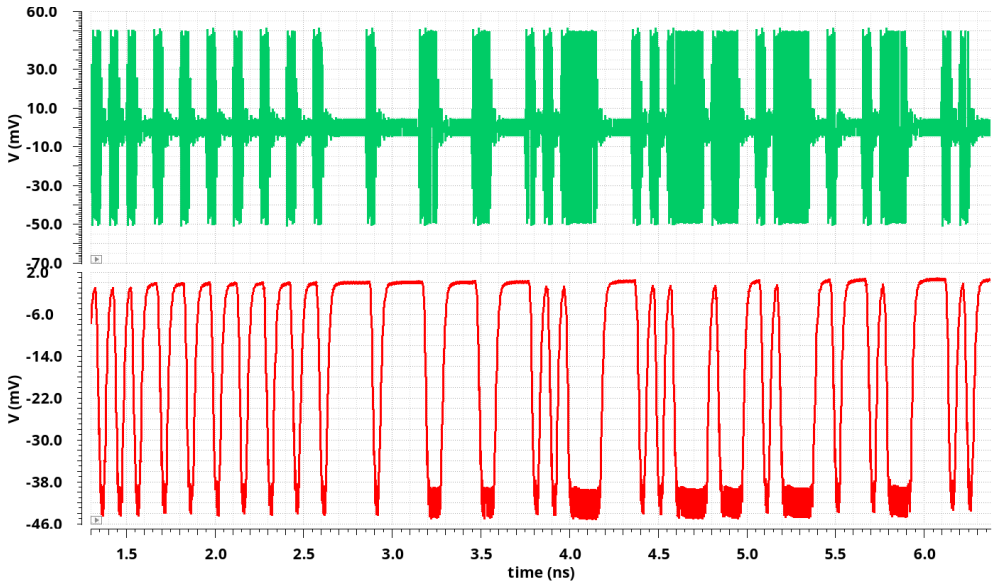

Figure 4.14: Simulated input and corresponding output from the PD, using a carrier of 130 GHz and a data rate of 20 Gbps.

The change in output voltage for different input power levels were measured. As input a D-band VDI extender WR-6.5 was used, which was calibrated using the corresponding VDI calibration kit, and verified using an Erickson power meter (PM5), VDI. The output voltage was measured using a voltage meter. The voltage change for different input powers, both simulated and measured can be seen in Fig. 4.15.

The LO leakage was measured by applying 0 dBm input power, and sweeping the frequency between 110 GHz and 170 GHz. The LO isolation of the signal was measured and is displayed in Fig. 4.16.

The DC power consumption of the PD is 59 mW, where the amplifier uses 55 mW.

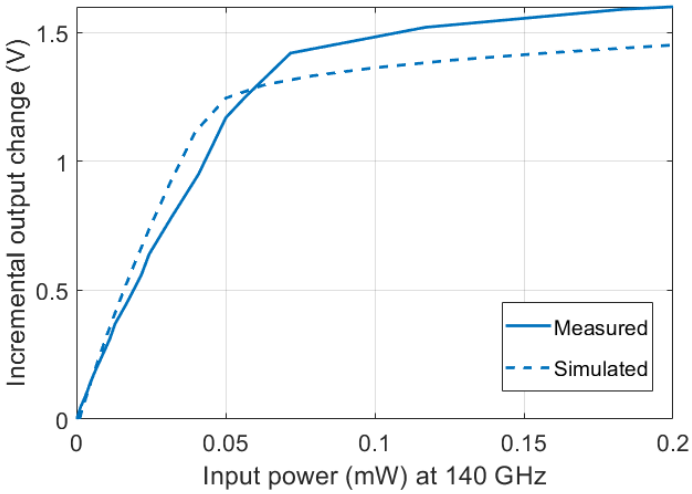

Figure 4.15: Difference in output voltage for different input powers (W). The dashed lines represent the simulated values, and the solid lines is the measured values.

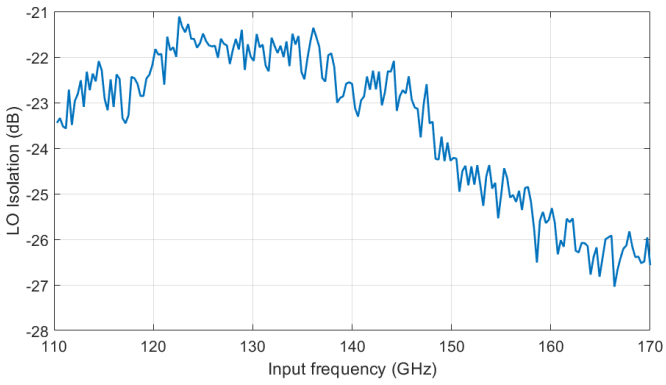

Figure 4.16: Isolation of the fundamental frequency measured at 0 dBm input power.

Chapter 5

Evaluation of the Communication Systems

In Paper C and Paper D transmitters and receivers were tested together during link measurements.

5.1 Tx/Rx in 250 nm InP DHBT Technology

The F-band "emitter coupled pair"-based RF-DAC (section 4.3) was used as a transmitter in the link. The PD receiver used an active balun at the input. A photo of the PD can be seen in 5.1.

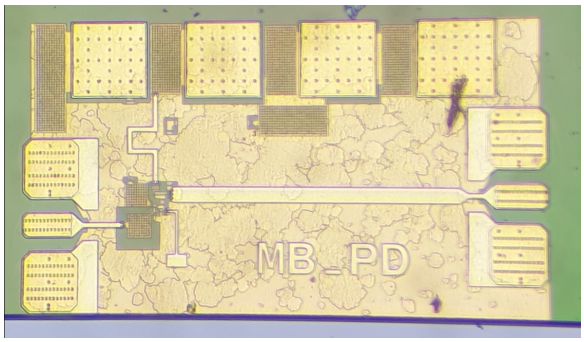

Figure 5.1: The PD used during the link measurements. The chip size including pads is 700 μm by 400 μm. Courtesy: Mingquan Bao

The link was tested in time domain transferring data in real time. The one meter PMF from Lehrstuhl für Hochfrequenztechnik (LHFT), was used to connect the circuits.

The output from the PD was connected a using coaxial cable to a Lecroy LabMaster 10-100Zi real-time oscilloscope where the signal could be analyzed. A photo of the fiber connecting the circuits on each probe station can be seen in Fig. 5.2.

The LO input signal for the RF-DAC was provided by a VDI vector network analyser (VNA) through an extender WR 6.5. The LO input frequency was set to 130.6 GHz, which together with the probe loss results in an input power of

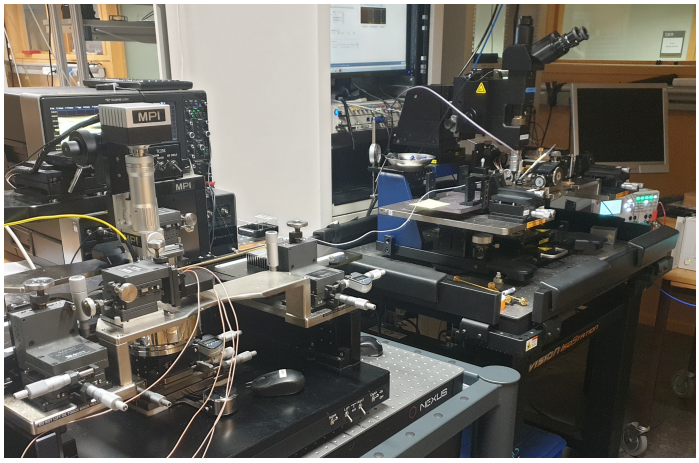

Figure 5.2: The setup that was used in the PMF link measurements. The fiber can be seen connecting one circuit on one probe station to the other one on the other probe station.

approximately -1.5 dBm delivered at the input of the RF-DAC. The data input was provided by a Keysight M8195A arbitrary waveform generator (AWG).

First the PMF link was tested using only one data input (MSB) to create a PAM-2 modulated signal. Bit rates up to 32 Gbps was measured and the data input that was used was a PRBS-9 stream. The eye diagram of the output signal from the PD can be seen in Fig. 5.3 (a) for a 30 Gbps signal and in Fig. 5.3 (b) for a 32 Gbps signal. For a 32 Gbps signal the bit error rate (BER) was 2.6×10^{-10}.

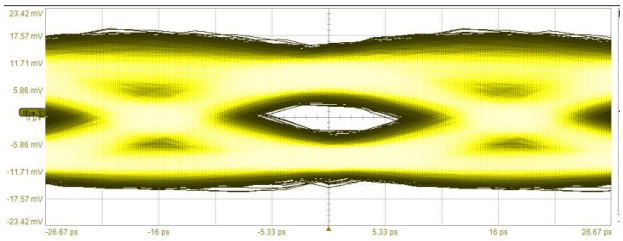

(a) 30 Gbps signal. BER $< \times 10^{-12}$

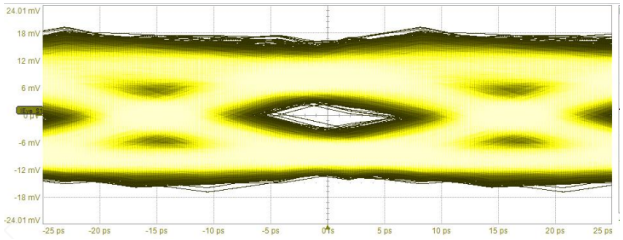

(b) 32 Gbps signal. BER $= 2.6 \times 10^{-10}$

Figure 5.3: Eyediagrams from the demodulated PAM-2 signal at 130.6 GHz.

For the PAM-4 PMF link measurements a PRBS-9 stream was used at the MSB data port and a PRBS-10 stream was used at the LSB data port. Data rates up to 15 GBaud was tested, corresponding to 30 Gbps. For 30 Gbps PAM-4 transmission the BER was 4.3×10^{-10}. Eyediagrams of the measurements can be seen in Fig. 5.4.

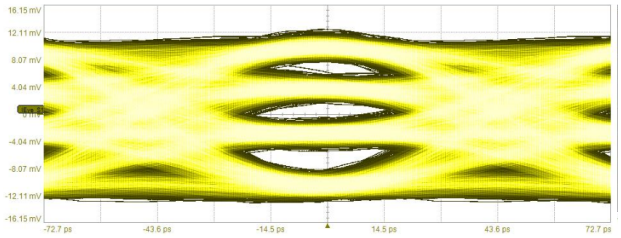

(a) 11 GBaud signal. BER $< 10^{-12}$

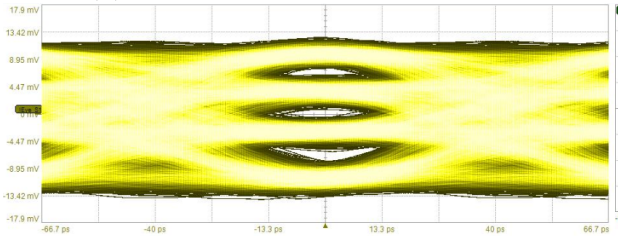

(b) 12 GBaud signal. BER $= 2.8 \times 10^{-12}$

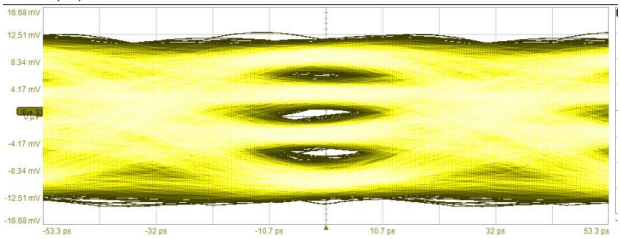

(c) 15 GBaud signal. BER $= 4.3 \times 10^{-10}$

Figure 5.4: Eyediagrams from the demodulated PAM-4 signal.

The total DC power consumption for the PMF link was measured to be 123 mW, which results in a energy efficiency of 4.1 pJ/bit for a 30 Gbps data transmission.

5.2 Tx/Rx in 130 nm SiGe BiCMOS Technology

The "stacked" RF-DAC was used as a transmitter. It included a frequency multiplier at the LO input and an amplifier at the output. A block diagram of the RF-DAC can be seen in 5.5.

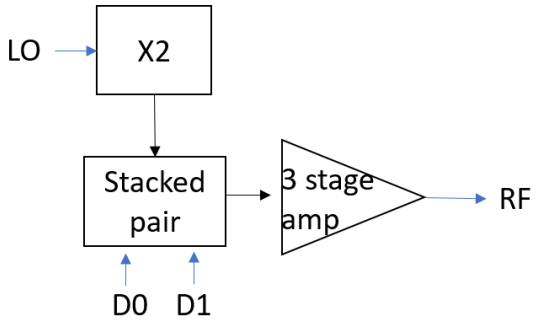

Figure 5.5: Block diagram of the RF-DAC.

The fabricated RF-DAC is depicted Fig. 5.6. The circuit is supplied by two DC bias of 2 V and 3 V. The size of the circuit is 1.18x0.72 mm^2 including pads.

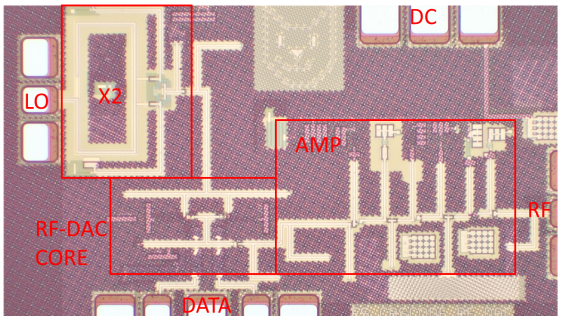

Figure 5.6: Photograph of the RF-DAC.

Same PMF, oscilloscope and AWG as in previous link measurement was used in this measurement. A photo of the fiber connecting the circuits on each probe station can be seen in Fig. 5.7.

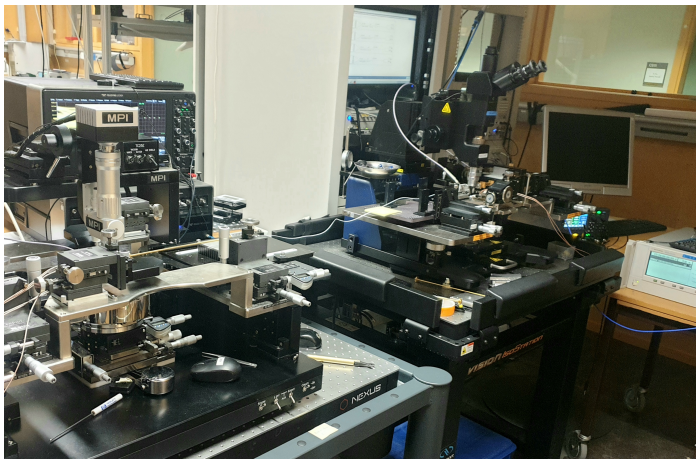

Figure 5.7: Setup that was used during the link measurement.

The LO input signal for the RF-DAC was provided by a signal generator (PSG 20 GHz Agilent E8257D) through a VDI extender WR-12. The LO input frequency was set to 69 GHz, resulting in a center RF-frequency of 138 GHz. Two pseudorandom binary sequences (PRBS-9 and PRBS-10) was provided by the AWG to generate the data. Different combinations of pulse shaping of the input stream, by the AWG, and equalization of the output stream, by the oscilloscope, were used. The equalizer is a Finite Impulse Response (FIR) equalizer, using 21 taps [14]. An external DC block was used at the output of the PD during all measurements.

In Fig. 5.8 eye diagrams of the output can be seen, using a carrier frequency of 138 GHz. Figure 5.8 A, both root-raised cosine (RRC) pulse shaping, with a roll-off factor of 1, and de-emphasis (DE) with one -5 dB post-cursor tap was used. Equalization (FIR with 21 taps) is used at the output. Figure B uses the same pulse shaping as Figure A, but without equalization at the output. Figure C uses no pulse shaping of the input bit stream, but equalization at the output of the PD. Datarates

are 10 Gbaud (20 Gbps), 9 Gbaud (18 Gbps) and 8 Gbaud (16 Gbps), and the bit error rate (BER) of the transmissions are less than 10^{-12}.

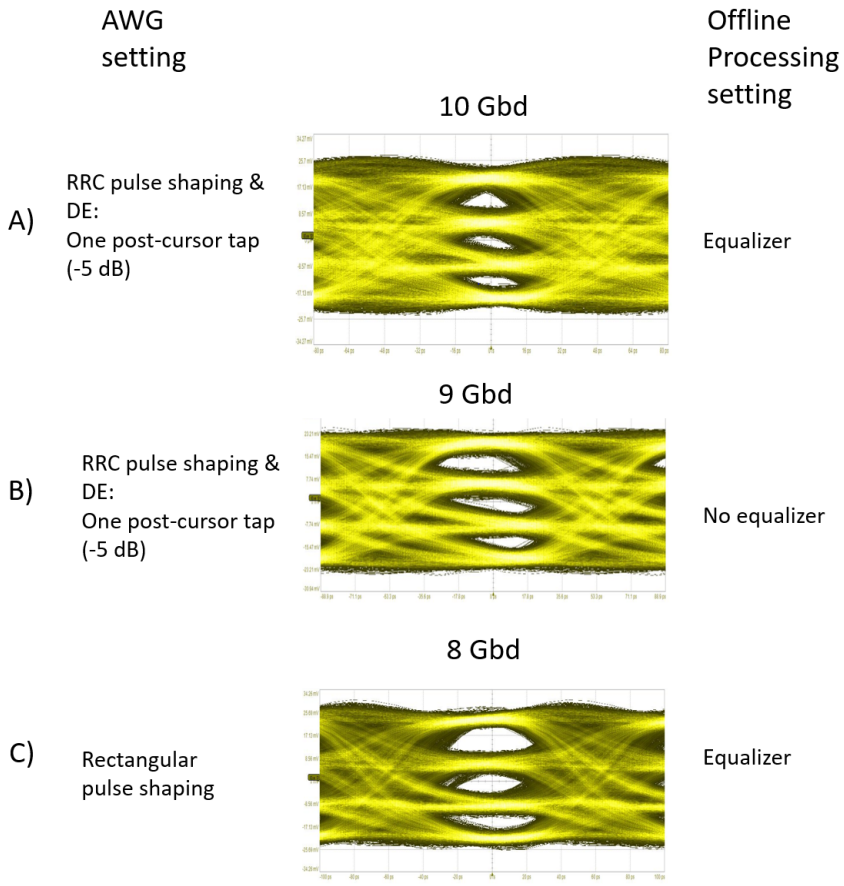

Figure 5.8: Eye diagrams of the output from the PD at 69 GHz LO (138 GHz RF) for A) 10 Gbaud using RRC pulse shaping and DE with one -5 dB post-cursor tap. Equalization is also used at output. B) 9 Gbaud using RRC pulse shaping and DE with one -5 dB post-cursor tap. C) 8 Gbaud with no pulse shaping, but equalization is used at output. All transmissions have a BER $< 10^{-12}$.

In Fig. 5.9, eye diagrams for baud rates between 6 Gbaud and 4 Gbaud, corresponding to 12 Gbps and 8 Gbps, are shown. No equalization was used at the output of the PD, and all transmissions have a BER $< 10^{-12}$. In Figure D, de-emphasis with one -5 dB post-cursor tap is used, while in Figure E, de-emphasis with one -3 dB post-cursor tap is used. In Figure F, RRC pulse shaping with a roll-off factor of 1 is used. In Figure G, no pulse shaping (rectangular) is used of the input bit stream.

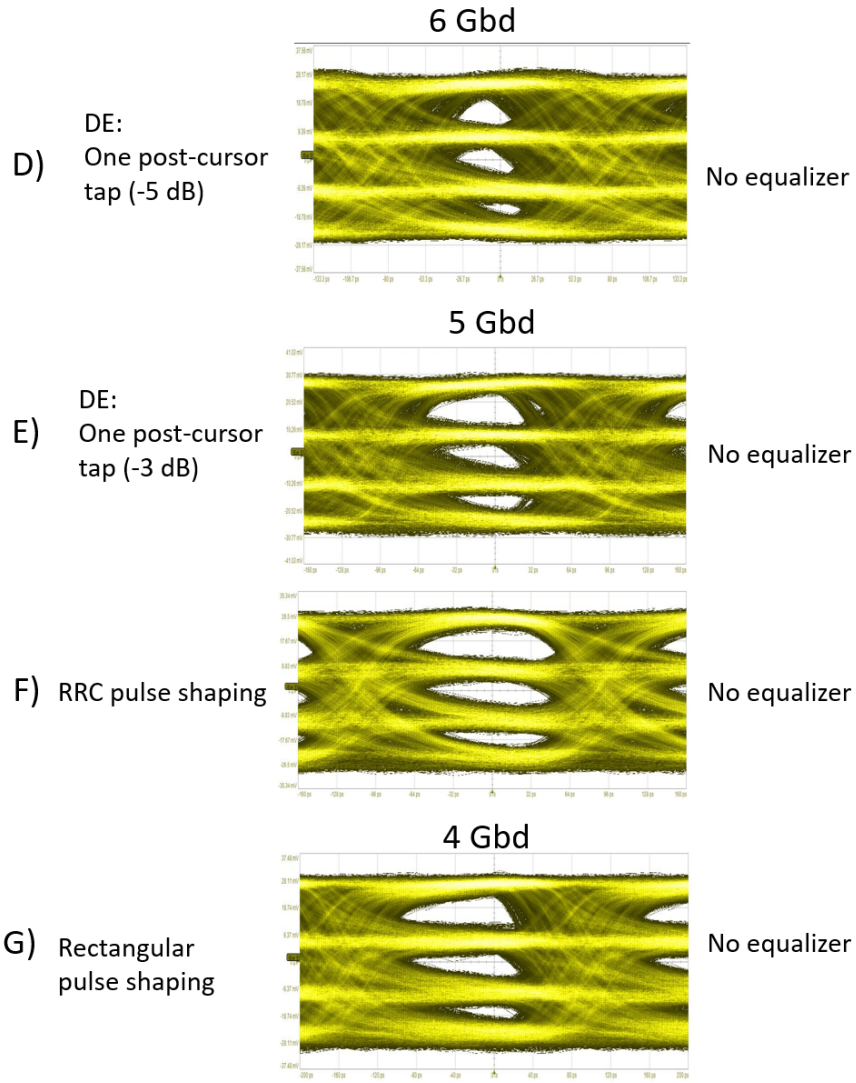

Figure 5.9: Eye diagrams of the output from the PD at 69 GHz LO (138 GHz RF) for D) 6 Gbaud using DE with one -5 dB post-cursor tap. E) 5 Gbaud using DE with one -3 dB post-cursor tap. F) 5 Gbaud using RRC pulse shaping. G) 4 Gbaud with no pulse shaping. All transmissions have a BER $< 10^{-12}$.

5.3 Comparison with similar work

In Table 5.1 the performance of a few similar links are presented. In Table 5.2 the performance of the links in this work is presented for comparison.

Compared to the works in 5.1, data rate and chip area are significantly superior. The energy efficiency is competitive, though since no on-chip LO is used, it is not easy to compare. Further more, for the PAM-4 systems to be complete, there should be a single bitstream at the output, and in these circuits the output is in PAM-4.

Table 5.1: Comparison with other links, with BER $< 10^{-12}$

Ref.	[17]	[4]	[8]
Technology	40 nm CMOS	28 nm CMOS	65 nm CMOS
Modulation	CP-FSK	CP-FSK	ASK
Frequency (GHz)	120	140	60
Data Rate (Gbps)	17.7	12	6
Fiber Length (m)	1.0	1.0	2.0
Energy Eff. (pJ/bit) *no LO included	4.0*	19.2	4.7
Total chip area (mm^2)	N/A	2.31	N/A

Table 5.2: Links in this work, with BER $< 10^{-12}$

Ref.	C	C	D
Technology	250nm InP DHBT	250nm InP DHBT	130nm BiCMOS
Modulation	PAM-2	PAM-4	PAM-4
Frequency (GHz)	131	131	138
Data Rate (Gbps)	30	22	20
Fiber Length (m)	1.0	1.0	1.0
Energy Eff. (pJ/bit) *no LO included	4.1*	5.6*	9.55*
Total chip area (mm^2)	0.83	0.83	1.54

Chapter 6

Conclusion and Future work

6.1 Conclusion

In this work, different solutions for high data rate communication have been presented. The emitter coupled RF-DAC has demonstrated great potential for speed, while the stacked topology was a strong competitor for its low dc power consumption.

The topologies investigated for the PDs were based on using baluns at the input to suppress the fundamental frequency. Both passive and active baluns were tested.

The RF-DAC based transmitters and PDs have demonstrated up to 30 Gbps error free (BER$<10^{-12}$) data transmissions in real time.

More understanding of the effects of the PMF on a PAM-modulated signal, provided insights that a higher carrier frequency (compared to what was used in these links) is desirable for broadband signals.

6.2 Future work

Future work include further development of the RF-DAC/PD PMF communication link, to reach a datarate of 100 Gbps. The plan is to move up in frequency to G-band (140 GHz - 220 GHz). Areas to focus on is bandwidth, power consumption and output power. Integration of more components, like comparators at the receiver, to be able to get a bitstream as output. Further exploring options on how to deal with the effects of the fiber on the signal.

Bibliography

[1] M. Bao, J. Chen, R. Kozhuharov, and H. Zirath. "14 Gbps on-off keying modulator and demodulator for D-band communication". In: *Proc. IEEE Int. Wireless Symp. (IWS 2014)*. Mar. 2014, pp. 1–4. DOI: 10.1109/IEEE-IWS.2014.6864208 (cit. on p. 25).

[2] M. A. Bhagyaveni, R. Kalidoss, and K. S. Vishvaksenan. *Introduction to analog and digital communication*. 2016 (cit. on p. 2).

[3] Kai Chang. *RF and Microwave Wireless Systems*. 2000. DOI: 10.1002/0471224324 (cit. on p. 6).

[4] M. De Wit, Y. Zhang, and P. Reynaert. "Analysis and Design of a Foam-Cladded PMF Link With Phase Tuning in 28-nm CMOS". In: *IEEE Journal of Solid-State Circuits* 54.7 (July 2019), pp. 1960–1969. ISSN: 1558-173X. DOI: 10.1109/JSSC.2019.2907163 (cit. on p. 37).

[5] Ke Lin Du and M. N.S. Swamy. *Wireless communication systems: From RF subsystems to 4G enabling technologies*. 2010. DOI: 10.1017/CBO9780511841453 (cit. on p. 9).

[6] Jonathan Hacker, Miguel Urteaga, Munkyo Seo, Anders Skalare, and Robert Lin. "InP HBT amplifier MMICs operating to 0.67 THz". In: 2013. DOI: 10.1109/MWSYM.2013.6697518 (cit. on p. 2).

[7] Clement J. *Internet usage worldwide - Statistics Facts | Statista*. 2020. URL: https://www.statista.com/topics/1145/internet-usage-worldwide/ (cit. on p. 1).

[8] Y. Kim, L. Nan, J. Cong, and M. F. Chang. "High-Speed mm-Wave Data-Link Based on Hollow Plastic Cable and CMOS Transceiver". In: *IEEE Microwave and Wireless Components Letters* 23.12 (Dec. 2013), pp. 674–676. ISSN: 1558-1764. DOI: 10.1109/LMWC.2013.2283862 (cit. on p. 37).

[9] R. R. Mahmud, M. A.G. Khan, and S. M.A. Razzak. "Design of a duobinary encoder and decoder circuits for communication systems". In: 2010. DOI: 10.1109/ICELCE.2010.5700550 (cit. on p. 22).

[10] Sanaz Mortazavi, Detlef Schleicher, and Friedel Gerfers. "Modeling and Verification of Automotive Multi-Gig Ethernet Communication up to 2.5 Gbps and the Corresponding EMC Analysis". In: 2018. ISBN: 9781538666210. DOI: 10.1109/EMCSI.2018.8495375 (cit. on p. 22).

[11] Hyunsu Park, Junyoung Song, Yeonho Lee, Jincheol Sim, Jonghyuck Choi, and Chulwoo Kim. "23.3 A 3-bit/2UI 27Gb/s PAM-3 Single-Ended Transceiver Using One-Tap DFE for Next-Generation Memory Interface". In: vol. 2019-February. 2019. DOI: 10.1109/ISSCC.2019.8662462 (cit. on p. 22).

[12] P. Reynaert, M. Tytgat, W. Volkaerts, A. Standaert, Y. Zhang, M. De Wit, and N. Van Thienen. "Polymer Microwave Fibers: A blend of RF, copper and optical communication". In: *Proc. ESSCIRC Conf. 2016: 42nd European Solid-State Circuits Conf.* Sept. 2016, pp. 15–20. DOI: 10.1109/ESSCIRC.2016.7598233 (cit. on p. 19).

[13] Patrick Reynaert, Kristof Dens, Carl D'Heer, Dragan Simic, Joren Vaes, Bart Philippe, and Simon Ooms. "Polymer microwave fiber: A new communication concept that blends wireless, wireline and optical communication". In: 2019. DOI: 10.1109/ICECS46596.2019.8964776 (cit. on p. 7).

[14] Inc. Teledyne LeCroy. *Instruction Manual - VectorLinQ - Vector Signal Analysis Software*. 2016. URL: http://cdn.teledynelecroy.com/files/manuals/vectorlinq-software-instruction-manual.pdf (cit. on p. 34).

[15] M. Tytgat and P. Reynaert. "A plastic waveguide receiver in 40nm CMOS with on-chip bondwire antenna". In: *Proc. ESSCIRC (ESSCIRC) 2013*. Sept. 2013, pp. 335–338. DOI: 10.1109/ESSCIRC.2013.6649141 (cit. on p. 19).

[16] N. Van Thienen, W. Volkaerts, and P. Reynaert. "A Multi-Gigabit CPFSK Polymer Microwave Fiber Communication Link in 40 nm CMOS". In: *IEEE Journal of Solid-State Circuits* 51.8 (Aug. 2016), pp. 1952–1958. ISSN: 1558-173X. DOI: 10.1109/JSSC.2016.2580605 (cit. on p. 19).

[17] N. Van Thienen, Y. Zhang, M. De Wit, and P. Reynaert. "An 18Gbps polymer microwave fiber (PMF) communication link in 40nm CMOS". In: *Proc. ESSCIRC Conf. 2016: 42nd European Solid-State Circuits Conf.* Sept. 2016, pp. 483–486. DOI: 10.1109/ESSCIRC.2016.7598346 (cit. on p. 37).

[18] Sorin Voinigescu. *High-Frequency Integrated Circuits*. 2013. DOI: 10.1017/cbo9781139021128 (cit. on p. 19).

[19] W. Volkaerts, N. Van Thienen, and P. Reynaert. "10.2 An FSK plastic waveguide communication link in 40nm CMOS". In: *Proc. IEEE Int. Solid-State Circuits Conf. - (ISSCC) Digest of Technical Papers*. Feb. 2015, pp. 1–3. DOI: 10.1109/ISSCC.2015.7062984 (cit. on p. 19).

Acknowledgments

First and foremost, I would like to thank Prof. Herbert Zirath and Assoc. Prof. Zhongxia Simon He. Without your enormous patience, inspiration and support this work would not have been possible. You really understand my passion for circuit design.

I would like to thank Assoc. Prof. Dan Kuylenstierna for giving me new challenges, and Dr. Mingquan Bao for sharing some of his knowledge. I would also like to thank Prof. Jan Stake for his support. Assoc. Prof Vessen Vassilev is always an inspiration even though I don't really work with you.

My gratitude also goes to Infineon Technologies and Teledyne Scientic Company for fabrication of the circuits (that are used in this thesis).

To my colleagues and friends; Ahmed, Olivier, Ibrahim, Sining, Stavros, Martin, Juan, José, Thanh, Yu as well as many more, you truly make my days better. I am thankful that you guys still put up with me.

Last but not least, I would like to thank my family, as well as my cat Mufasa and my horses. You always make me keep going. From horse riding I have learned that even if you fall, it's not a failure unless you give up.

Frida Strömbeck
Göteborg, March 2021